CLYC versus Stilbene: Optimization and comparison of two neutron-gamma discriminating scintillators

Stephen Asztalos Wolfgang Hennig

Abstract–CLYC is a novel scintillator with excellent pulse shape discrimination attributes. When introducing a new scintillator it is helpful to derive a quantitative measure of its performance. A detailed analysis is performed with CLYC and another common material Stilbene - two materials capable of neutron/photon discrimination. Using one particular choice of a figure of merit we find that CLYC outspecifies Stilbene by a factor of 50.

I. Introduction

Recent developments in neutron detection materials have yielded a new class of Li-based compounds such as Cs_2LiYCl_6:Ce (CLYC) [1], which not only exhibits excellent pulse shape discrimination (PSD) but also good energy resolution. CLYC is in a class of Li-based epasolite scintillators that detects thermal neutrons by virtue of the reaction $n + {}^6Li \rightarrow {}^3H + {}^4He$, with the reaction products carrying away ~ 4.8 MeV. That PSD capability and good energy resolution coexist in the same material sets it apart from most scintillators. The timing of these developments is especially fortuitous as there is documented global shortage of ^3He [2] - the working gas in the ubiquitous ^3He neutron detector - caused mainly by growing needs for neutron detectors in national security, nonproliferation, defense, border security, and homeland security applications.

II. Digital Pulse Shape Analysis

To characterize CLYC material and thus derive a better understanding of its PSD capability we acquired and analyzed an extensive data set taken at Lawrence Berkeley National Laboratory using an XIA digital P500 spectrometer. The specific objectives of this run were: 1) to optimize CLYC performance using an XIA digital filtering algorithm developed for phoswich applications, 2) to test the ability of the XIA 500 MHz P500 ADC to resolve CLYC's previously described fast (intrinsic sub-ns) photon emission and 3) to compare CLYC performance with that of Stilbene under identical test conditions.The experimental setup consisted of a 56 mCi AmBe source to produce a mixed neutron-gamma radiation field, a 2" CLYC crystal (RMD) coupled to a Photonis X2020 photomultiplier tube (PMT) and an identical PMT coupled to a 2" packaged cylinder of the liquid scintillator Stilbene. The two PMTs were nearly in direct opposition and approximately 18" of paraffin separated each PMT from the source to moderate fast neutrons. Approximately 50M event traces were acquired in each data stream over the course of the several day run. XIA's digital filtering algorithms permit online or offline computation of running filter sums. For optimal energy resolution a trapezoidal energy filter is customary (though its length can be adjusted to optimize energy resolution). In the present analysis energy resolution is is less important, so an running integral energy filter sum of length *E* was used instead. Filters used specifically for pulse shape analysis (PSA) historically are less well-established. In previous and present analyses a fast running filter sum of length *LP* is placed some variable distance LoP beyond the trigger location, where fast refers to sufficiently short to capture high frequency behavior. We define the filter sums *A* and *B*, using filters of length *LP* and *E*, respectively as

$$\sum_{LP} n_i = A; \sum_{E} n_i = B,$$

where n_i to the number of counts in channel *i*. Fig. 1 shows a typical CLYC traces with the various filter parameters illustrated.

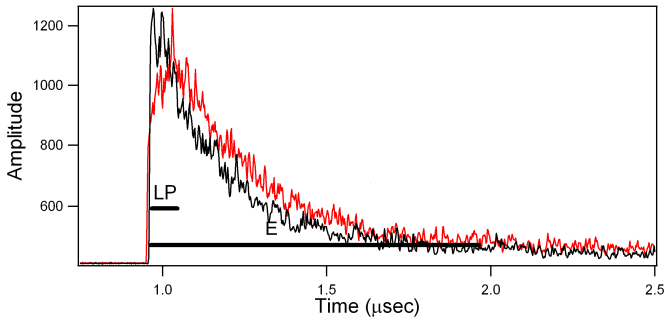

Man uscript received November 21, 2010.
S. Asztalos is with XIA LLC Hayward, CA 94554 (telephone: 510-401-5760, e-mail: steve@xia.com).
W. Hennig is with XIA LLC Hayward, CA 94554 (telephone: 510-401-5760, e-mail: whennig@xia.com).

Fig. 1. overlays two distinct traces from CLYC data acquired with an AmBe source and the XIA P500 spectrometer. In this figure the black trace is seen to have a somewhat shorter smaller rise time than the red trace. Digital filters of length *LP* and *E* are shown in this figure.

To differentiate the transient behavior of these two traces appropriate choices of *LP* and *E* are made. The right graph in Fig. 2 plots *B* as a function of the ratio *A/B* over a restricted *A/B* interval for one particular value of *LP*. With *LP* appropriately chosen *A/B* should be somewhat smaller for the red than the black trace in Fig. 1. This is precisely the behavior seen in the right graph in Fig. 2: data with low *A/B* values and tightly clustered values of *B* are all found to resemble the red trace in Fig. 1, while data with higher *A/B* values and widely distributed values for *B* are all self-similar to the black trace.

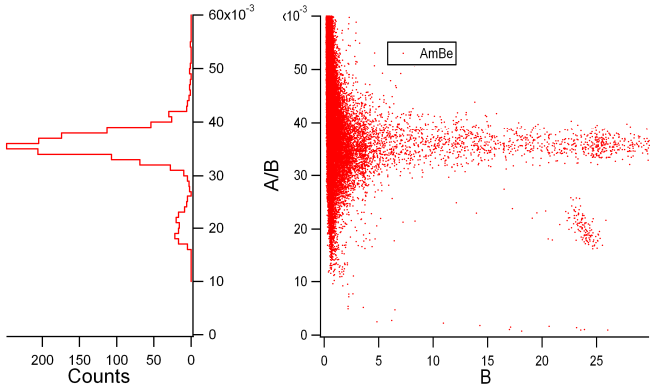

Fig. 2. (Right) A discrimination plot from CLYC data acquired with an AmBe source and the P500 spectrometer. For this plot *LoP* was set at 0 ns, *LP* 36 ns and *E* 2.016 us. (Left) A projection of the discrimination plot onto the *A/B* axis.

The left graph in Fig. 2 is a projection of the right graph onto the *A/B* axis with the restriction that *B* exceed 5. This projection cleanly separates the events into two distinct distributions. By varying *LP* the separation between the two distributions, hence, the discrimination (specificity) can be optimized.

III. Pulse Shape Discrimination with CLYC

Before proceeding with the details of our CLYC analysis a brief discussion of its properties is warranted. CLYC is a representative of a class of related epasolite materials, including $Cs_2LiLaCl_6$ (CLLC) and $Cs_2LiLaBr_6$ (CLLB), each with excellent PSD capabilities. (Neither CLLB and CLLC will be commercially available for the foreseeable future, but may be available for research purposes). In all of these Li-based materials thermal neutrons are detected via the nuclear reaction $n+^6Li \rightarrow {}^3H+{}^4He$ that imparts ~ 4.8 MeV to the reaction products. These charged, recoiling reaction products induce scintillation in a traditional manner, though quenching of the heavy charged recoils leads to less light output and, hence, smaller equivalent energy deposition (roughly 3.2 MeV photon equivalent). Thermal neutrons interacting with CLYC produce about 60,000 photons (around 20,000 photons/MeV) [3]. Naturally occurring Li is found in present CLYC samples, though it has recently been shown that the concentration of ^6Li can be increased to 80-90% [4], hence, improving neutron efficiency. As is customary with new scintillator materials, this excellent light yield energy resolution was obtained with only with a small CLYC sample. Larger (1") samples have demonstrated excellent PSD capabilities, as well. Crystals as large as 2" in diameter have already been grown [4]. several day run. More limited runs were taken with the paraffin removed, alternative geometries and a ^{137}Cs source. In what follows we describe preliminary results from our analyses of this data. It merits emphasizing the preliminary aspect of these analysis as CLYC has numerous and, perhaps, yet undescribed decay mechanisms and whose ultimate performance may require optimization of other parameters (e.g., ADC sampling rate, rise time and threshold cuts) not considered below.

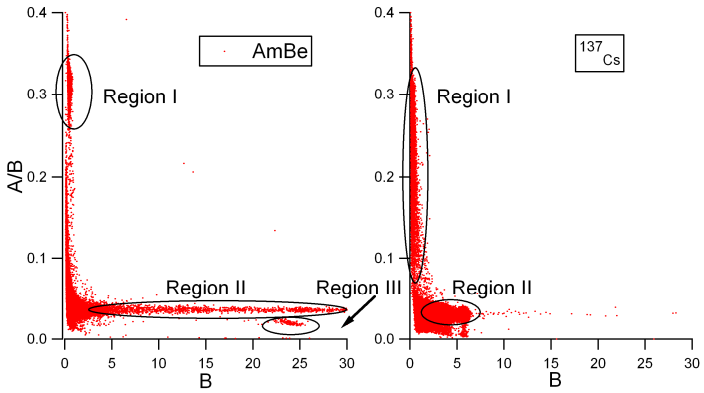

Fig. 3. (Left) The ratio A/B versus B for CLYC using an AmBe source. (Right) Same, but using a ^{137}Cs source .

The left graph in Fig. 3 shows *A/B* as a function of *B* from CLYC data acquired with an AmBe source over the entire range of data. The right plot shows the same but taken with a ^{137}Cs source. The data in Fig. 3 acquired with an AmBe source now reveals three distinct regions of interest. Selected events from these three regions are shown in Fig. 4.

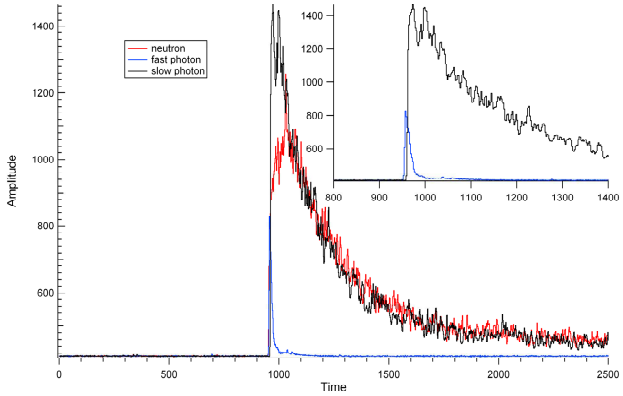

Fig. 4. Selected fast (blue), slow photon (black) and neutron (red) events from CLYC data acquired with an AmBe source. The inset compares fast and slow photon pulse shapes.

The blue trace in Fig. 4 is representative of events from Region I (large A/B - low B values) seen in both the AmBe and ^{137}Cs data sets. These events have been described in the literature and are ascribed to the phenomenon of Core-to-Valence-Luminescence which underlies the intrinsic sub-nanosecond rise and decay times. This type of emission has been shown to appear only under gamma excitation, and only a few known materials are known that exhibit it [5]. The response of the PMT and the analog Nyquist filter of the P500 slow the rise time to a few ns, while competing de-excitation processes result in the observed ~ 65 ns and ~ 1000 ns decay components. The black trace is representative of events from Region II (low B/A values and widely varying B values) also seen in both the AmBe and ^{137}Cs data sets. The black trace exhibits a somewhat shorter rise time than that of the red trace, although the decay times are quite similar. The slight differences in kinetics between slow photon and neutron events may arise from the differing ionization densities of the recoiling electron in the former versus that of the recoiling ^{3}H and ^{4}He ions in the latter. Further, these data suggest, though it is far from established, that some subset of the slow photon events may better described as an admixture fast and slow of photon mechanisms. Further studies are needed to confirm or refute this hypothesis. The red trace is a representative event from Region III (low A/B - large B values). The absence of similar traces in CLYC data taken with a ^{137}Cs source and their energy equivalent of 3.2 MeV from the ^{137}Cs calibration strongly suggests their identification as neutron events. This trace exhibits a rise time of ~ 40 ns and a single decay component of ~ 620 ns - kinetics similar to those described in the literature and likewise ascribed to neutrons. Such events are thought to be understood in terms of the energy transfer from the host to the Ce^{3+} ion [5]. The red and black traces in Fig. 1 can now be positively associated with neutron and photon events, respectively.

In proceeding with a quantitative description of CLYC specificity, the bottom graph in Fig. 5 shows a total projection onto the *A/B* axis of data from the left graph (AmBe data) in Fig. 3. The two upper graphs likewise are projections of Fig. 3 but after the indicated energy cuts have been imposed.

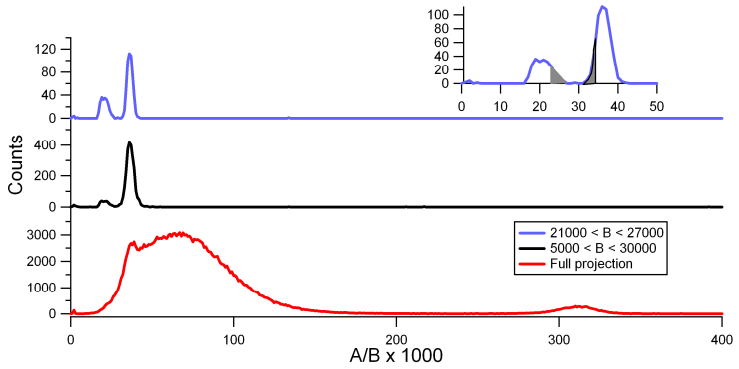

Fig. 5. A total projection of the data from Fig. 3 along the y-axis and two projections subject to the indicated energy cuts.

There are at least two ways in which the specificity can be improved: either the trigger threshold can be increased to eliminate low energy events (events along a constant *A/B* minus *B* line) or, alternatively, an energy cut can be imposed. The latter alternative was chosen for this analysis. The top two plots in Fig. 5 are the result of applying energy cuts as indicated in the figure legend. The top graph is generated from an energy window in the vicinity of the neutron cluster in Fig. 3. Although the middle plot demonstrates that the energy cut can be quite generous while still maintaining excellent specificity, in subsequent analysis the tight energy cut is used primarily to facilitate analysis of the Stilbene data, where these same projections are much broader due to its poor energy resolution and lack of a localized neutron response. To optimize the specificity of CLYC and Stilbene, the filter length *LP* was varied from 0 to 60 ns (in increments of 2 ns) and applied offline to the list mode data containing the raw waveforms. For each value of *LP* a projection similar to Fig. 5 was made and the mean bin computed to separate neutron from photon peaks, which were each fit to a Gaussian distribution. A figure of merit (FOM) was constructed by computing the area between + (-) 3 sigma of the peaks' centroids to the end of the neutron (gamma) spectrum (see inset in Fig. 5 for an illustration). The absolute value of each was computed (fits of the Gaussian tails occasionally dip below the x-axis) and summed to define the FOM. (Here a small value for the FOM implies better specificity.) This definition of the FOM emphasizes counts between the neutron and gamma peaks hence, specificity, as opposed to their widths or separations found in more traditional definitions. The FOMs for CLYC and Stilbene are plotted in Fig. 6 as a function of *LP*.

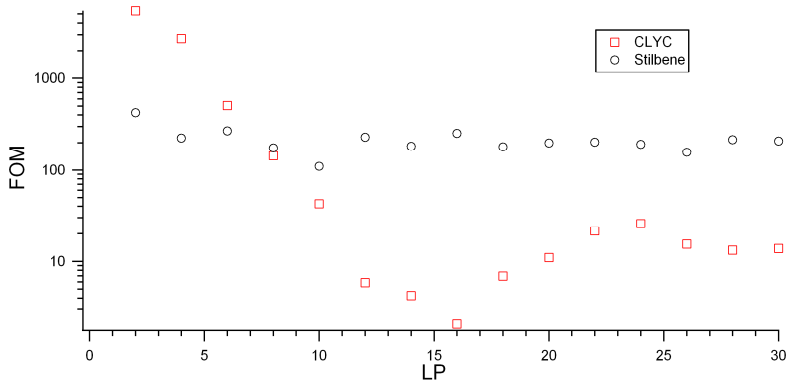

Fig. 6. FOM (as defined in the text and Fig. 5 inset) as a function of *LP* for CLYC and Stilbene data. *LoP* is zero for all *LP*.

The plot shows that CLYC has a rather well defined minimum between a filter length *LP* of 12 and 18, while Stilbene has no well defined minimum. For its optimal filter length of 16 CLYC has a FOM of 2 and for a representative filter length of 10 Stilbene an FOM of 110. Fig. 7 overlays the projections of the CLYC and Stilbene data for the chosen filter lengths. Note the absence of counts between the neutron and photon peaks in this statistics-limited CLYC data set.

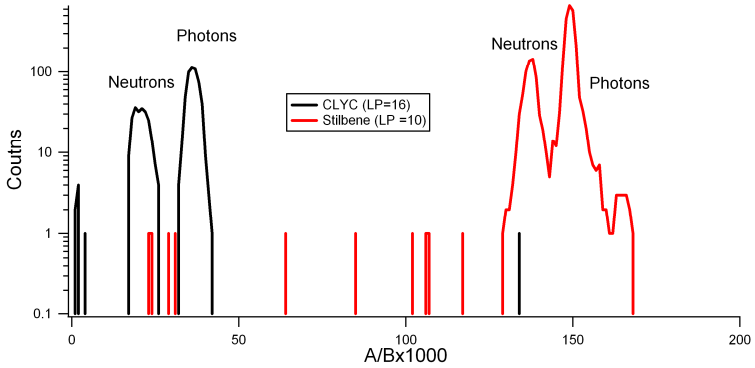

Fig. 7. Projections of CLYC and Stilbene data for the chosen filter lengths.

Using this particular choice of optimization one can state that CLYC outspecifies Stilbene by a factor of ~ 50. Loosening the energy cut will somewhat degrade the FOM, though the onset is more rapid in Stilbene than CLYC.

IV. Conclusions

Questions concerning the neutron/gamma specificity of CLYC pulse shapes have been partially answered by a direct comparison with Stilbene - a conventional liquid scintillator noted for its neutron/gamma specificity. We have demonstrated that CLYC's performance as a neutron/gamma detector can be improved by optimizing a single analysis parameter related to the early behavior of the pulse shape. We find that in this limited optimized analysis CLYC outperforms Stilbene by a factor of 50 or more. Further, CLYC reportedly delivers excellent energy resolution (~ 4.5%) [6], though to achieve this result requires a matched PMT and wider integral sum. Undoubtedly the PSD performance of CLYC could be improved by considering other PSA parameters.

Acknowledgment

We wish to acknowledge the staff (Paul Fallon and Larry Phair) at the 88” cyclotron at LBNL for use of the facilities and sources for our CLYC measurements.

References

[1] A. Bessiere, et al., NIM A, Volume 537, Issues 1-2 (2005) p. 242; J. Glodo, et al., IEEE Trans. Nucl. Sci., Volume 56, Issue 3 (2009), p. 1257
[2] R.T. Kouzes, The ^{3}He Supply Problem, PNNL Report 18388 (2009)
[3] J. Glodo, et al, 2007 IEEE Nuc. Sci. Symp. Rec 2, (2007), p. 959
[4] Presentation by RMD at the IEEE Nuc. Sci Symp, Knoxville (2009) (unpublished).
[5] Ibid 3.
[6] Ibid 1.
[7] Ibid 2.
[8] E. Van Loef, et al., J. Phys.: Condens. Matter, Volume 14, (2002), p. 8481
[9] Ibid 2.